

EUROFEL-Report-2007-DS2-045

EUROPEAN FEL Design Study



Deliverable N°: D 2.13

Deliverable Title: Development of the code HOMDYN, and applications to the beam dynamics of photo-injectors like SPARC with comparisons to experimental measurements

Task: DS-2

Authors: V. Fusco

Contract N°: 011935

**Project funded by the European Community
under the “Structuring the European Research Area” Specific Programme
Research Infrastructures action**

DEVELOPMENT OF THE HOMDYN CODE AND APPLICATIONS TO THE BEAM DYNAMICS OF THE PHOTO- INJECTORS LIKE SPARC WITH COMPARISONS TO EXPERIMENTAL MEASUREMENTS*

V. FUSCO[†]

*LNF-INFN, Via E. Fermi 40,
00044 Frascati, Italia*

Wake fields effects in addition to space charge forces may have an important impact during the emittance compensation process in a high brightness photo-injector. To study this effect we developed an upgraded version of the Homdyn code including off axis beam dynamics and wake fields.

Homdyn describes a bunch as a uniformly charged cylinder, divided in cylindrical slices; in the upgraded version each slice's centroid can be transversally displaced from the nominal axis thus inducing wake fields. When the bunch is short as compared to the beam pipe radius, wake fields for a single cavity are calculated using methods of diffraction theory; instead we use, for a periodic collection of cavities, an asymptotic wake field obtained numerically at SLAC and then fitted to a simple function.

As a first application we studied a correction scheme for the SPARC photo-injector to control the bunch trajectory and angle at the entrance of the undulator. The correction scheme consists of a number of steering magnets and beam position monitors placed along the photo-injector. Two different steering approaches are analyzed and the emittance degradation is studied. The code demonstrates the steering positions and number do correct the bunch's orbit and angle and gives good results concerning the emittance degradation.

Finally we show comparisons between the SPARC e-meter measurements and Homdyn simulations.

* Work partially supported by the EU Commissioning in the sixth frame-work programme, contract no 011935 EURO-FEL-DS2

[†] valeria.fusco@lnf.infn.it

1. Introduction

Good performances of a free electron laser depend on the quality of the beam at the entrance of the undulator. To achieve short radiation wavelength and short gain length we need a high brightness beam that is a high current and a low emittance beam.

During the propagation of a beam through a photo-injector, the beam may experience emittance growth. Emittance degradation is due to space charge and RF fields non linearities and longitudinal correlation along the bunch induced by transverse space charge, transverse RF fields and transverse wake fields.

Figure 1 represents the bunch in the phase space when the longitudinal correlation is induced along the bunch. The bunch has been divided into slices; each one is subject to a different transverse force, due to the space charge field, the RF field and the wake field, so each slice fills a different oriented area in the phase space assuming as a whole a fan shape. The consequence is that even if the emittance of each slice is preserved (if only linear forces are acting), the emittance over the whole bunch is not preserved.

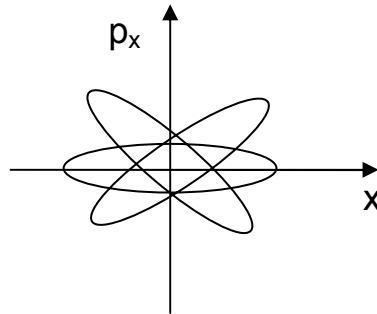


Figure 1. Fan shape of the emittance due to transverse fields induced by correlation along the bunch.

2. The Homdyn Model

Because wake fields may have an important impact during the space charge emittance compensation process [1], the Homdyn code has been developed to include off axis beam dynamics.

The Homdyn code [2] is a fast semi-analytical code whose main approximation consists in supposing the bunch as a uniformly charged cylinder. The cylinder is divided in slices whose evolution is described by differential equations for the envelopes and the centroids [3].

When the bunch is traveling on the axis each slice can evolve as in Figure 2a, that is after a time Δt each slice's radius and length can change under the space charge, the RF force, the solenoid force and eventually the length of the bunch can change also under the longitudinal wake field force. Anyway the slice's centroid can't be displaced from the axis and the bunch has to travel along the main axis.

The improvement is depicted in Figure 2b [4]: after a time Δt each slice's radius and length can change and moreover the slice's centroid can be displaced from the nominal axis.

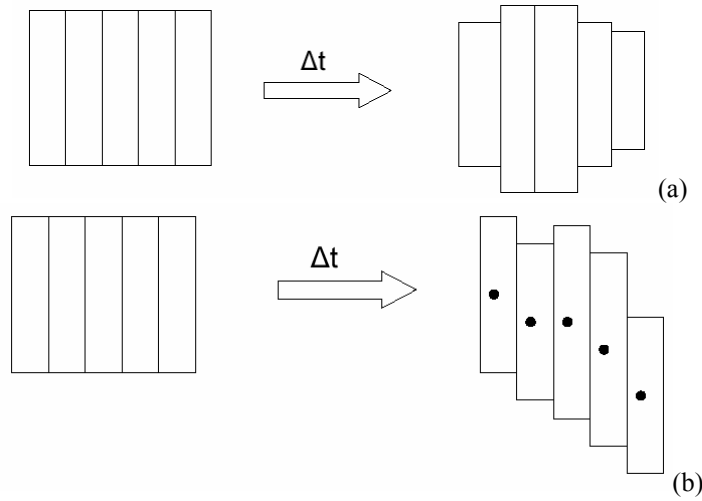


Figure 2. Multi-slice approximation in the Homdyn code: when the bunch is traveling on axis (a) and when it is traveling off axis (b).

The envelope equations for each slice of a bunch are:

$$\begin{aligned} \ddot{x}_s + \beta_s \gamma_s^2 \dot{\beta}_s \dot{x}_s + (k_s^{rf} + k_s^{sol})^2 x_s &= \frac{e}{\gamma_s^3 m} E_x^{sc}(\xi_s, A_s) + \left(\frac{4\mathcal{E}_n^{th}}{\gamma_s} \right)^2 \frac{1}{x_s^3} \\ \ddot{y}_s + \beta_s \gamma_s^2 \dot{\beta}_s \dot{y}_s + (k_s^{rf} + k_s^{sol})^2 y_s &= \frac{e}{\gamma_s^3 m} E_y^{sc}(\xi_s, A_s) + \left(\frac{4\mathcal{E}_n^{th}}{\gamma_s} \right)^2 \frac{1}{y_s^3}. \end{aligned} \quad (1)$$

where x_s and y_s are the single slice's radius, whilst the centroids motion for each slice traveling on the axis is simply represented by the following differential equation:

$$\begin{aligned}\ddot{z}_s &= \dot{\beta}_s c \\ \dot{\beta}_s &= \frac{e}{mc\gamma_s^3} E_z^{sc}(\xi_s, A_s) + \frac{e}{mc\gamma} \left[E_z^{rf}(z_{cs}, t) + E_{\parallel}^w(\xi_s) \right]\end{aligned}\quad (2)$$

where e is the electron charge, m the electron rest mass and c the speed of light.

It is worth noting no off axis motion is included but only a longitudinal motion represented by z_s .

The Lorentz contraction factor for each slice is γ_s , being $\gamma_s = 1/(1-\beta_s^2)^{1/2}$. The RF focusing gradient for each slice is [2]:

$$k_s^{rf} = \frac{e}{2\gamma_s m} \left(\frac{\partial E_z^{rf}}{\partial z} + \frac{\beta_s}{c} \frac{\partial E_z^{rf}}{\partial t} \right). \quad (3)$$

expressed through the linear expansion off-axis of the accelerating field $E_z^{rf}(z_s, t)$, the solenoid focusing gradient is:

$$k_s^{sol} = \left(\frac{eB_z(z_s)}{2\gamma_s m} \right)^2. \quad (4)$$

The transverse and longitudinal space charge is represented by the terms $E_x^{sc}(\xi_s, A_s)$, $E_y^{sc}(\xi_s, A_s)$ and $E_z^{sc}(\xi_s, A_s)$ respectively where $\xi_s = z_s - z_t$ and z_t is the position of the bunch's tail, A_s is the aspect ratio defined as $A_s = R/\gamma_s L_s$ where R is the radius of the bunch section [5] and L_s is the slice length. Finally in Eq. (2) the last term on the right hand side, $E_{\parallel}^w(\xi_s)$, represents the longitudinal wake fields (see section 3).

When the bunch is traveling off axis, the differential equations for the slice's centroids transverse motion are:

$$\begin{aligned}\ddot{x}_c + \beta\gamma^2 \dot{\beta} \dot{x}_c + k_s^{rf} x_c &= \frac{e}{\gamma_s^3 m} E_x^{sc}(\xi_s, A_s, d_{xc}) + \frac{e}{\gamma m} E_{\perp}^w(\xi_s, x_{cs}) \\ \ddot{y}_c + \beta\gamma^2 \dot{\beta} \dot{y}_c + k_s^{rf} y_c &= \frac{e}{\gamma_s^3 m} E_y^{sc}(\xi_s, A_s, d_{yc}) + \frac{e}{\gamma m} E_{\perp}^w(\xi_s, y_{cs})\end{aligned}\quad (5)$$

As shown in Eq. (5) besides the RF field, each slice centroid can experience transverse wake fields, $E_{\perp}(\xi_s, x_{cs})$ (illustrated in section 3), and transverse space charge fields, $E_x^{sc}(\xi_s, A_s, d_{xc})$ and $E_y^{sc}(\xi_s, A_s, d_{yc})$, due to neighbor slices displaced d_{xc} or d_{yc} from the considered slice. It's worth noting Eq. (5), which is similar to Eq. (1), doesn't include the emittance term since there's no emittance pressure acting on the slice's centroid.

3. Wake Fields in the Homdyn Model

Let's consider a point charge Q (the leading charge) and a test charge q (the trailing charge) situated behind Q . If the charges are moving in an enclosed space and the conducting wall has a non zero resistivity or the devices have wall discontinuities, the electromagnetic field generated by the leading charge is scattered by the wall thus affecting the trailing charge [5]. These electromagnetic fields are called wake fields since, from causality, the leading charge cannot affect itself nor any charge in front of it but only charges lying behind it.

As a consequence an accelerator device whose shape is not uniform induces longitudinal wake fields and when the devices are misaligned respect to a nominal axis or the bunch is traveling off axis it induces transverse wake fields. Transverse wake fields contribute to emittance degradation.

We distinguish the case the bunch travels along a single cavity and a periodic collection of cavities.

3.1. Single Cavity

When the bunch's length σ is much smaller than the beam pipe radius a , $\sigma \ll a$, methods of diffraction theory [6] are used to calculate the impedance at high frequencies, $\omega \gg c/a$, where c is the speed of light. The model suppose each structure as a pill box cavity, whose geometric dimensions are: a the beam pipe radius, b the cavity radius and g its length. When a bunch reaches the edge of the cavity, the electromagnetic field is just the one that would occur when a plane wave passes trough a hole; with this hypothesis it is possible to use the classical diffraction theory of optics to calculate the fields.

According to it, the longitudinal and transverse wake potential are respectively [7]:

$$\begin{aligned}
W_{\parallel 0}(s) &= \frac{Z_0 c}{\sqrt{2\pi^2 a}} \sqrt{\frac{g}{s}} \\
W_{\perp 0}(s) &= \frac{2^{3/2} Z_0 c}{\pi^2 a^3} \sqrt{gs}.
\end{aligned} \tag{6}$$

where Z_0 is the characteristic impedance and s the longitudinal coordinate inside the bunch, being $s=0$ the bunch's head.

Eq. (6) are the fields produced by a point charge on a test charge at a distance s : they represent Green functions. One can calculate the longitudinal and transverse wake potential of an arbitrary distribution by making the convolution of the bunch distribution with the Green functions.

For a uniformly charged cylinder, as the one considered in Homdyn, we can obtain the wake potential and finally the wake fields to be inserted in Eq. (2) and Eq. (5) [8]:

$$\begin{aligned}
E_{\parallel}^w(s) &= \frac{q}{L} \frac{2}{\sqrt{2\pi^2 a \epsilon_0}} \sqrt{\frac{s}{g}} \\
E_{\perp}^w(s, x) &= \frac{q}{L} \frac{2^{5/2}}{3\pi^2 a^3 \epsilon_0} \frac{s^{3/2}}{\sqrt{g}} x
\end{aligned} \tag{7}$$

where q is the bunch's charge, L its length and x is the bunch's head displacement from the nominal axis, having supposed the other slices' displacement do not differ much from the head.

It's worth noting that both the longitudinal and transverse wakes do not depend on the cavity radius b . Infact part of the diffracted field, generated when the leading edge of the bunch enters the cavity, will propagate in the cavity; if the bunch's rms length σ is shorter than the cavity radius b , then the geometrical condition $g < (b-a)^2/2\sigma$ is verified and the scattered field coming from the upper wall of the cavity will never reach the tail of the bunch itself: this is called cavity regime.

3.2. Periodic Structures

For a collection of cavities, Eq. (6) can't be used anymore because the wake fields, along the cavities, do not sum in phase and the result would be an overestimation of the effects. An asymptotic wake field, for a periodic collection of cavities of period p , obtained numerically at SLAC [9] and then fitted to a

simple function is used instead. Such wake field is thus valid after a certain number of cavities given by [10]:

$$N_{crit} = \frac{a^2}{2g\left(\sigma + \frac{2a}{\gamma}\right)} \quad (8)$$

The Green functions are:

$$\begin{aligned} W_{\parallel 0}(s) &= \frac{Z_0 c}{\pi a^2} e^{-\sqrt{s/s_1}} \\ W_{\perp 0}(s) &= \frac{4Z_0 c s_2}{\pi a^4} \left[1 - \left(1 + \sqrt{\frac{s}{s_2}} \right) e^{-\sqrt{s/s_2}} \right]. \end{aligned} \quad (9)$$

where:

$$\begin{aligned} s_1 &= 0.41 \frac{a^{1.8} g^{1.6}}{p^{2.4}} \\ s_2 &= 0.17 \frac{a^{1.79} g^{0.38}}{p^{1.17}}. \end{aligned} \quad (10)$$

Eq. (9) are valid when $s/p \leq 0.15$, $0.34 \leq a/p \leq 0.69$ and $0.54 \leq g/p \leq 0.89$. Such constraints are fulfilled for the SLAC cavities used in SPARC where $a=11.6 \text{ mm}$, $g=29.2 \text{ mm}$ and $p=35.0 \text{ mm}$.

Following the same procedure of a single cavity one can obtain [11] the longitudinal and transverse wake potential from the Green functions and thus the wake fields for a uniform charge distribution:

$$\begin{aligned} E_{\parallel}^{win}(s) &= \frac{2Z_0 c s_1 q}{\pi a^2 L} \left[1 - e^{-\sqrt{s/s_1}} \left(1 + \sqrt{\frac{s}{s_1}} \right) \right] \\ E_{\perp}^{win}(s, x) &= \frac{4Z_0 c s_2^2 q x}{\pi a^4 L} \left[-6 + \frac{s}{s_2} + 2e^{-\sqrt{s/s_2}} \left(3 + 3\sqrt{\frac{s}{s_2}} + \frac{s}{s_2} \right) \right]. \end{aligned} \quad (11)$$

Eq. (11) can be inserted in Eq. (2) and Eq. (5). In this case the displacement x is, as for the single cavity, the offset of the first slice.

Anyway to obtain a better evaluation of the beam dynamics due to wake fields, the fields to be inserted in Eq. (2) and Eq. (5) can be obtained as the superposition of the wake fields generated by the single slices with x the single's slice offset. The wake fields generated outside a bunch, that is when $s > L$, are:

$$E_{\parallel}^{w,out}(s) = \frac{2Z_0 c s_1 q}{\pi \alpha^2 L} \left[e^{-\sqrt{(s-L)/s_1}} \left(1 + \sqrt{\frac{s-L}{s_1}} \right) - e^{-\sqrt{s/s_1}} \left(1 + \sqrt{\frac{s}{s_1}} \right) \right]$$

$$E_{\perp}^{w,out}(s, x) = \frac{4Z_0 c s_2^2 q x}{\pi \alpha^4 L} \left[\begin{aligned} & \frac{L}{s_2} + 2e^{-\sqrt{s/s_2}} \left(3 + 3\sqrt{\frac{s}{s_2}} + \frac{s}{s_2} \right) + \\ & - 2e^{-\sqrt{(s-L)/s_2}} \left(3 + 3\sqrt{\frac{s-L}{s_2}} + \frac{s-L}{s_2} \right) \end{aligned} \right]. \quad (12)$$

As illustrated in Figure 3 each slice generates a longitudinal and a transverse wake field. The fields inside the slices (Eq. (11)) and outside the slices (Eq. (12)) sum up to give the whole field, the displacement x depending on the single slices offset. Thus the convoluted fields to be inserted in Eq. (2) and Eq. (5) are:

$$E_{\parallel}^w(s) = \sum_1^{N-N_s} \left[E_{\parallel i}^{w,out}(s) + E_{\parallel i=N_s}^{w,in}(s) \right] \quad (13)$$

$$E_{\perp}^w(s) = \sum_1^{N-N_s} \left[E_{\perp i}^{w,out}(s) + E_{\perp i=N_s}^{w,in}(s) \right] \quad (14)$$

where N_s is the considered slice number.

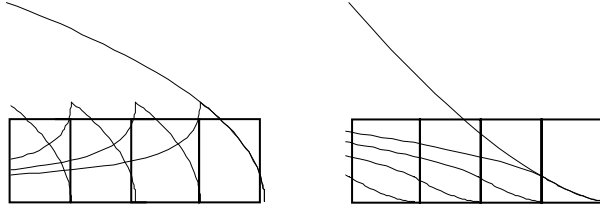


Figure 3. Longitudinal (left hand side) and transverse (right hand side) wake field generated by single slices.

3.3. Energy spread and offset due to wake fields

The energy spread and the offset computed by Homdyn when wake fields are switched on have been compared with the energy spread and the offset calculated analytically for a single cavity and a periodic structure. The comparison is good thus the simple expressions obtained give the possibility to evaluate quickly the energy spread and the offset.

The energy spread is defined in Homdyn as:

$$\frac{\Delta\gamma}{\gamma} = \frac{\sqrt{\langle (\gamma - \langle \gamma \rangle)^2 \rangle}}{\langle \gamma \rangle}. \quad (15)$$

In the case the space charge and the RF fields are switched off in the code, the energy spread is only due to the longitudinal wake field thus:

$$\frac{\Delta E}{E_0} = \sigma_E = \frac{el_{str} \sqrt{\langle (E_{\parallel}^w(s) - \langle E_{\parallel}^w(s) \rangle)^2 \rangle}}{E_0}. \quad (16)$$

where e is the electron charge, E_0 is the average energy, $E_{\parallel}^w(s)$ is the longitudinal wake field per unit length of the path of a single cavity (Eq. (7)) or a periodic structure (Eq. (11), Eq. (13) and Eq. (14)) and l_{str} is the length of the structure where wake fields are acting. From Eq. (16) we have

$$\sigma_E^2 = \frac{e^2 l_{str}^2}{E_0^2 q} \int_{-\infty}^{+\infty} \lambda(s) (E_{\parallel}^w(s) - \langle E_{\parallel}^w(s) \rangle)^2 ds \quad (17)$$

and

$$\langle E_{\parallel}^w(s) \rangle = \frac{1}{q} \int_{-\infty}^{+\infty} \lambda(s) E_{\parallel}^w(s) ds = k_{\parallel} \quad (18)$$

With k_{\parallel} we introduce the average energy loss, the so called loss factor. In our treatment the loss factor is measured as V/m . Solving Eq. (17) we obtain:

$$\sigma_E^2 = \frac{e^2 l_{str}^2}{E_0^2} \left[\frac{1}{L} \int_0^L (E_{\parallel}^w(s))^2 ds - k_{\parallel}^2 \right] \quad (19)$$

Introducing the fields for a single cavity or a periodic structure we can solve Eq. (19). For a single cavity we obtain a very simple expression here shown:

$$\sigma_E = \frac{1}{3} \left(\frac{Z_0 c q}{\pi^2 a} \right) \sqrt{\frac{1}{g L}} \frac{e l_{str}}{E_0} \quad (20)$$

In the case of the transverse wake fields we can evaluate their effects considering the transverse offset given to the bunch. Using Eq. (5) in the time domain, we obtain :

$$\langle x_c \rangle \cong \frac{k_{\perp}}{\gamma m c^2 / e} \frac{l_{str}^2}{2 \beta^2} + x_c'(0) z + x_c(0) \quad (21)$$

Where $x_c'(0)$ and $x_c(0)$ are the initial angle and offset respectively and

$$k_{\perp} = \frac{1}{q} \int_{-\infty}^{+\infty} \lambda(s) E_{\perp}^w(s) ds \quad (22)$$

It's worth noting Eq. (21) has been derived supposing the offset of the slices is constant and equal to the offset of the first slice.

Inserting the transverse fields for a single cavity or a periodic structure we can solve Eq. (22). For a single cavity we have:

$$\langle x_c \rangle = \frac{e}{\beta^2 \gamma m c^2} \frac{2^{7/2}}{15} \frac{Z_0 c q x}{\pi^2 a^3} \sqrt{\frac{L}{g}} \frac{z^2}{2} \quad (23)$$

when $x_c'(0)=0$ and $x_c(0)=0$.

Such analytical calculations have been compared with the results computed by the Homdyn code for the energy spread and the transverse offset.

Table 1 summarizes the energy spread, $\Delta\gamma/\gamma$, and the offset, x_c , for a single cavity of the SLAC type, as computed by Homdyn and by the analytical calculation, versus the average energy, E_0 , of the bunch.

Table 2, as for a single cavity, gives the energy spread and the offset for a periodic structure of the SLAC type, versus the average energy of the bunch as computed by Homdyn and by the analytical calculation.

Finally we evaluate the approximation made in Homdyn to calculate the effects of the transverse wake fields when we only consider the offset of the first slice compared to the case, described in the preceding section, when every slice offset is considered in Homdyn and the fields, both longitudinal and transverse, are obtained as a superposition of the fields generated by the single slices.

Table 1. Energy spread in percent, $\Delta\gamma/\gamma\%$, and offset, x_c , versus the bunch's average energy, E_0 , for a single cavity obtained with the analytic calculation and as computed by the Homdyn code.

E_0 [MeV]	$\Delta\gamma/\gamma\%$		x_c [mm]	
	Homdyn	Analytic	Homdyn	Analytic
1	0.07	0.10	$6.3 \cdot 10^{-4}$	$5.6 \cdot 10^{-4}$
3	0.029	0.034	$2.1 \cdot 10^{-4}$	$2.1 \cdot 10^{-4}$
5	0.019	0.021	$1.4 \cdot 10^{-4}$	$1.4 \cdot 10^{-4}$
9	0.011	0.011	$0.87 \cdot 10^{-4}$	$0.80 \cdot 10^{-4}$
30	0.0035	0.0034	$0.28 \cdot 10^{-4}$	$0.25 \cdot 10^{-4}$
50	0.0021	0.0021	$0.17 \cdot 10^{-4}$	$0.15 \cdot 10^{-4}$
70	0.0015	0.0015	$0.12 \cdot 10^{-4}$	$0.11 \cdot 10^{-4}$

Table 2. Energy spread in percent, $\Delta\gamma/\gamma\%$, and offset, x_c , versus the bunch's average energy, E_0 , for a periodic structure obtained with the analytic calculation and as computed by the Homdyn code.

E [MeV]	$\Delta\gamma/\gamma\%$		x_c [mm]	
	Homdyn	Analytic	Homdyn	Analytic
1	2.9	3.0	6.3	7.2
3	2.4	2.6	1.4	1.5
5	1.7	1.7	0.77	0.78
9	0.99	0.67	0.42	0.42
30	0.31	0.30	0.13	0.13
50	0.19	0.18	0.077	0.077
70	0.13	0.13	0.056	0.055

Table 3. Energy spread in percent, $\Delta\gamma/\gamma\%$, and offset, x_c , versus the bunch's average energy, E_0 , for a periodic structure obtained with and without wakefields convolution.

E [MeV]	$\Delta\gamma/\gamma\%$		x_c [mm]	
	Noconv	Conv	Noconv	Conv
1	2.9	3.5	6.3	7.9
3	2.4	2.5	1.4	1.5
5	1.68	1.69	0.77	0.90
9	0.99	0.99	0.42	0.50
30	0.31	0.31	0.13	0.15
50	0.19	0.18	0.077	0.091
70	0.13	0.13	0.055	0.065

This gives an estimation of the mistake made in the analytical calculation considering only the first slice's offset. Thus Table 3 compares the energy spread and the offset when Homdyn is used in the convolution configuration or not. The table demonstrates there is a little difference for the energy spread case whilst the difference increases for the offset case.

4. Emittance Computation

The total rms normalized emittance is calculated in the code following the normalized rms emittance definition [12]:

$$\mathcal{E}_{nx} = \langle (x - \langle x \rangle)^2 \rangle \langle (\beta\gamma x' - \langle \beta\gamma x' \rangle)^2 \rangle - \langle (x - \langle x \rangle)(\beta\gamma x' - \langle \beta\gamma x' \rangle) \rangle^2. \quad (24)$$

Such calculation is made following the code's approach which supposes the bunch divided in cylindrical slices.

Let's take S slices each containing M particles thus the whole bunch contains $N=M \cdot S$ particles. The media of Eq. (24) can be expanded in the following way:

$$\langle \rangle = \frac{1}{N} \sum_{n=1}^N [] = \frac{1}{S \cdot M} \sum_{s=1}^S \sum_{m=1}^M [] = \frac{1}{S} \sum_{s=1}^S \langle \rangle_s \quad (25)$$

For a uniform cylindrical charge distribution, the following relation holds:

$$\langle x^2 \rangle_s = \frac{X_s^2}{4} \quad (26)$$

and

$$\langle \frac{X_s^2}{4} \rangle = \frac{1}{S} \sum_{s=1}^S \frac{X_s^2}{4} \quad (27)$$

where X_s is the slice radius.

Solving Eq. (24) we obtain the following results: when all the slices lie on the same axis, the emittance is only given by the 'envelope' emittance

$$(\mathcal{E}_n^e)^2 = \langle \frac{X^2}{4} \rangle \langle \frac{p_x^2}{4} \rangle - \langle \frac{X p_x}{4} \rangle^2 \quad (28)$$

where we omitted the symbol s for the slice and $p_x = \beta\gamma dX/dz$ is the transverse momentum.

If the slices do not lie on the same axis then the emittance is not simply given by the envelope emittance but it is given by the quadratic sum of the envelope emittance and two more terms, the ‘centroids’ emittance

$$\begin{aligned} (\mathcal{E}_n^{cent})^2 = & \langle (x_c - \langle x_c \rangle)^2 \rangle \langle (p_{xc} - \langle p_{xc} \rangle)^2 \rangle + \\ & - \langle (x_c - \langle x_c \rangle)(p_{xc} - \langle p_{xc} \rangle) \rangle^2 \end{aligned} \quad (29)$$

and the ‘cross’ emittance

$$\begin{aligned} (\mathcal{E}_n^{cross})^2 = & \langle \frac{X^2}{4} \rangle \langle (p_{xc} - \langle p_{xc} \rangle)^2 \rangle + \\ & + \langle \frac{p_x^2}{4} \rangle \langle (x_c - \langle x_c \rangle)^2 \rangle + \\ & - 2 \langle \frac{Xp_x}{4} \rangle \langle (x_c - \langle x_c \rangle)(p_{xc} - \langle p_{xc} \rangle) \rangle \end{aligned} \quad (30)$$

Each slice’s envelope and each slice’s centroid can be represented in the phase space x , p_x and the spread of their distributions around their media represent the envelope emittance and the centroid emittance.

Let’s suppose the bunch has a zero envelope emittance that is the slice’s envelopes lie on a straight line as in Figure 4a and the centroid emittance is zero as well, being for example $p_{xc}=0$: this is represented in Figure 4b.

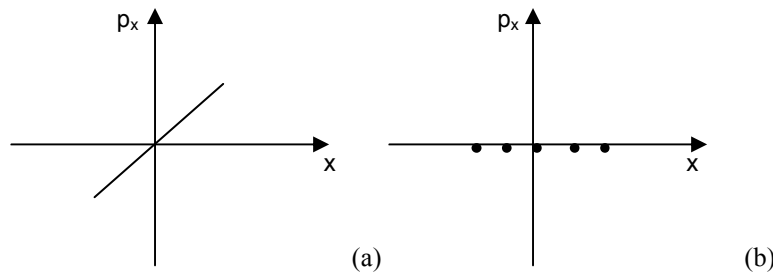


Figure 4. Slices’ envelope lying (dots) on a straight line (a) and slices’ centroids (dots) with $p_{xc}=0$

Nonetheless the cross emittance, thus the total emittance represented in Figure 5, can be different from zero, being from Eq. (30)

$$\left(\epsilon_n^{cross}\right)^2 = + \left\langle \frac{p_x^2}{4} \right\rangle \left\langle (x_c - \langle x_c \rangle)^2 \right\rangle \quad (31)$$

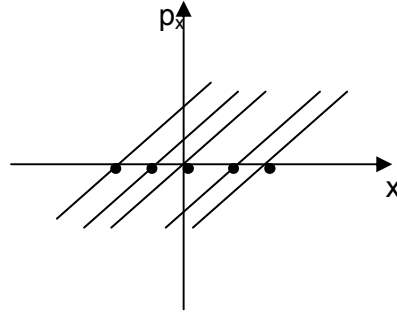


Figure 5. Cross emittance due to the distribution of the centroids and the envelopes of each slice.

The emittance complete expression of an off axis bunch has been inserted in the Homdyn code and it has been tested using the Parmela code [4].

5. Emittance Degradation Study in the SPARC Photo-injector

The SPARC project consists of a high brightness photo-injector for advanced accelerator experiments including a free electron laser. The whole device can be divided into two parts: the undulator devoted to the production of the radiation and the photo-injector whose aim is the production of a high quality electron beam to fulfill FEL requirements. Thus the Homdyn code, with its improvements on off axis beam dynamics has been used to study the bunch quality along the photo-injector until the entrance of the undulator.

The photo-injector consists of an electron source and accelerator sections.

The electron source for SPARC is a 1.6 cell RF gun operating at 2.856 GHz with a high peak field of 120 MV/m . The RF gun includes a metallic photocathode which is illuminated by a temporally flat, pico-second laser source. The system generates a 5.6 MeV electron beam which is accelerated to 155 MeV by three traveling wave sections of the SLAC type.

5.1. Misalignment correction scheme study in the SPARC traveling wave sections

A bunch can travel off axis for different reasons: for example a laser pointing instability can directly generate the bunch off axis or the structures can

be misaligned. In this case RF fields transverse components, space charge effects and transverse wake fields can further push the bunch off axis and increase the emittance. Thus the bunch has to be driven to the nominal trajectory with the help of steering magnets and beam position monitors (BPMs), placed along the accelerator structures.

To calculate the right angle in the vertical and horizontal plane that correct the trajectory, we use a transfer matrix between two points, for example the steering and the following BPMs or two adjacent steerings [3]

$$\begin{pmatrix} x \\ x' \\ y \\ y' \end{pmatrix}_2 = \begin{pmatrix} a & b & e & f \\ c & d & g & h \\ i & l & o & p \\ m & n & q & r \end{pmatrix} \begin{pmatrix} x \\ x' \\ y \\ y' \end{pmatrix}_1 \quad (32)$$

The matrix calculation is made up of two steps: the first step consists in the calculation of the matrix elements: we turn off the steering magnets, $x'=y'=0$, we obtain the nominal position on the following steering or BPM, x_{2n} and y_{2n}

$$\begin{cases} x_{2n} = ax_1 + ey_1 \\ y_{2n} = iy_1 + ox_1 \end{cases} \quad (33)$$

Turning on the horizontal steer we get the new positions x_{2k} and y_{2k}

$$\begin{cases} x_{2k} = x_{2n} + fy' \\ y_{2k} = y_{2n} + ly' \end{cases} \quad (34)$$

The second step determines the horizontal and vertical angle of the steering, being known the matrix element and the position wished on the following steer or BPM:

$$\begin{cases} bx' + y' = x_2 \\ px' + ly' = y_2 \end{cases} \quad (35)$$

It's worth noting such matrix determines the horizontal and vertical angle for one steering. The general case of more than one steering is solved using the superposition principle thus adding the contribution of each steering coming before the ending point.

The above treatment includes the case the horizontal and vertical plane are coupled, as in a solenoid magnetic field.

Figure 8 is a scheme of the steering magnets and the beam position monitors along the SPARC photo-injector: a steering is positioned just outside the gun, two in each traveling wave structure; one more at the end of the linac, after the focusing quadrupoles and finally the last one just before the undulator. Outside the linac, beam position monitors are placed after every steering whilst they are placed after every two steerings inside the linac structure.

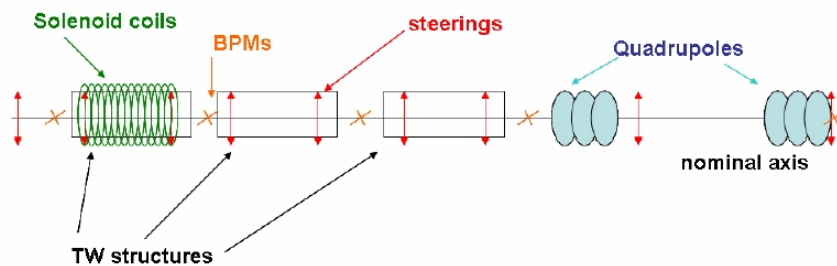


Figure 8. Steering magnets and beam position monitors positions in the SPARC photo-injector.

As a preliminary study of the emittance degradation, we analyze a case in which the bunch's centroid is driven further and further away from the nominal axis as shown in Figure 9.

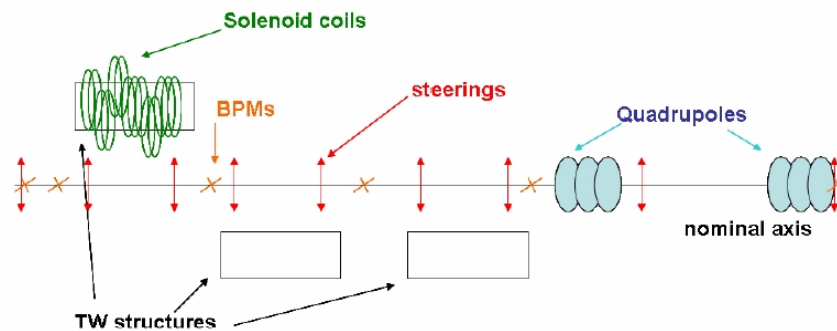


Figure 9. Traveling waves and solenoid coils misalignment in the SPARC photo-injector.

The bunch is generated on axis whilst the traveling waves can be transversally displaced with respect the nominal axis; besides, the thirteen coils forming the solenoid of the first traveling wave can be independently displaced as well: a study of different misaligned combinations of the solenoid coils shows

the worst configuration as concern the offset induced on the bunch. The configuration is summarized in Table 4.

To calculate the right angle in the vertical and horizontal plane that corrects the trajectory, the transfer matrix between two points has been used [4].

We first correct the misaligned configuration to drive the centroid trajectory back to the nominal axis. We use the Homdyn code as if we were simulating a virtual experiment; this means we try to align the bunch on the BPMs after each steering and we read the centroid position in the BPMs. Therefore only one steering before each BPMs is used.

Table 4. Solenoid coils' and TWs offset respect to the nominal axis.

Device	Δx mm	Δy mm
Solenoid coil 1	0.0	0.1
Solenoid coils 2-3-4-5-6	0.1	0.0
Solenoid coils 7-8-9-10-11-12-13	0.0	-0.1
TW1	0.1	0.1
TW2	-0.1	-0.1
TW3	-0.1	-0.1

The centroid position is successfully driven back to the nominal axis, anyway Table 5 shows an emittance which is not perfectly compensated. The reason is that even if the centroids travels back to the nominal axis, the traveling wave structures are misaligned thus the transverse wake fields exist and cause an emittance's growth that should be minimized.

Table 5. Horizontal and transverse emittance with and without steering correction when the bunch's centroid is driven back to the nominal axis.

ϵ_n	ϵ_{nx}	ϵ_{nx}	ϵ_{ny}	ϵ_{ny}
nominal	steer off	steer on	steer off	steer on
0.79 μm	2.95 μm	1.08 μm	1.12 μm	1.06 μm

Thus the technique used is the beam based alignment: it consists in forcing the bunch to undergo bumps and pass along the traveling wave axis as shown in Figure 10. Such technique uses all the steerings placed inside the linac instead of one per linac as in the previous case. We use again a transfer matrix to determine the steering angles.

Plots in Figure 11 represent the centroid trajectory with and without steering and demonstrate that the centroid travels on the axis of each traveling wave structure as in Figure 10. Finally Table 6 demonstrates the emittance obtained is perfectly compensated.

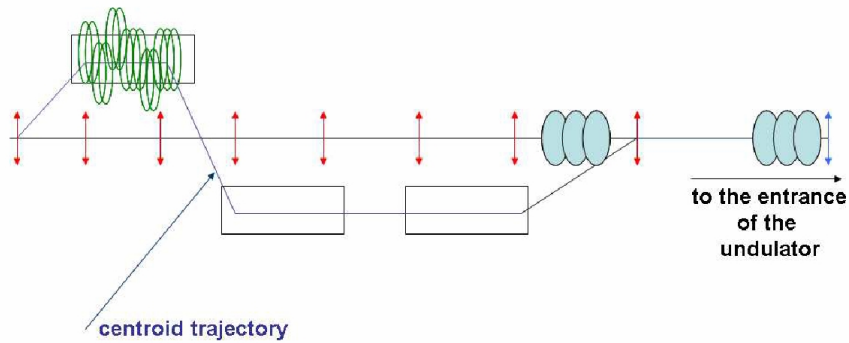


Figure 10. Centroid's trajectory along the linac with the beam based alignment technique.

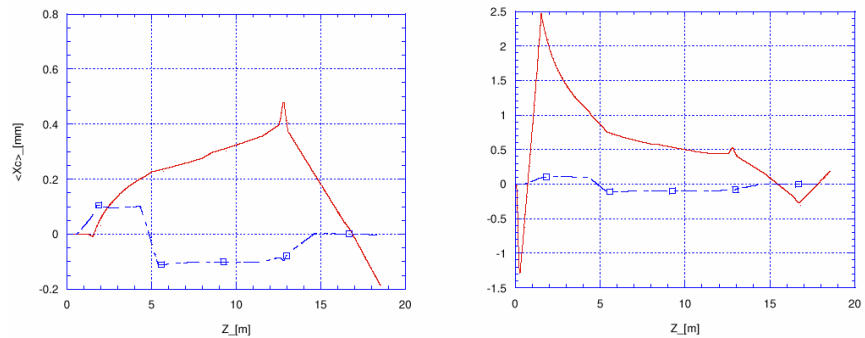


Figure 19. Horizontal and vertical centroid's trajectory along the linac using the bump technique with and without steering.

Table 6. Horizontal and transverse emittance with and without steering correction when the beam based alignment technique is used.

ϵ_n	ϵ_{nx}	ϵ_{nx}	ϵ_{ny}	ϵ_{ny}
nominal	steer off	steer on	steer off	steer on
0.79 μm	2.95 μm	0.79 μm	1.12 μm	0.79 μm

6. Comparisons between SPARC emittance-meter measurements and simulations with the Homdyn code

Before injecting the beam into the three accelerating sections, the beam has to be characterized and optimized at low energy (5 MeV) that is after the RF gun and the compensation solenoid. This is the first phase of the SPARC project.

Theoretically [13] by injecting a space charge dominated beam into accelerating sections when the so called invariant envelope condition is fulfilled, the emittance oscillation can be controlled and damped. Moreover if the beam is injected when the emittance is at its relative maximum (Ferrario working point), the emittance value at the linac exit is low and frozen to its local minimum. Infact the emittance performs the so called double minimum oscillation, a feature observed in simulations which characterizes this new working point, employed nowadays in photo-injectors worldwide.

To characterize the bunch evolution along the longitudinal coordinate z so that the beam can be properly matched to the booster, a new device, called emittance meter [14], was employed. The emittance meter is a movable device which can be moved thank to a bellow structure. Together with the rms spot size a system of horizontal and vertical slits allow the measure of the emittance and energy spread vs z .

6.1. Homdyn measurements comparisons

Most of comparisons between measurements and simulations have been performed, during the SPARC photo-injector commissioning, by the Parmela code [15]. As described above the reason is that, despite Homdyn is a very fast code, it has some intrinsic limit.

Thus the differences between the code and the measures are mainly due to the pulse rise/fall time, to the non perfect uniformity of the charge distribution and to the non linearity in the associated electromagnetic fields neglected by the code. Nonetheless it was interesting to compare Homdyn simulations and measures results as long as the agreement is quite satisfying.

As for Parmela a fitting procedure was anyway necessary [15]. The purpose was to keep the parameters value into the variation range established by the uncertainty of the measure itself. This was not always possible with Homdyn, depending on the shape of the pulse.

Different pulse shapes have been investigated emphasizing their different dynamics behavior in the emittance compensation process. The following figures show comparison between the beam envelope and emittance versus z for different pulse shapes.

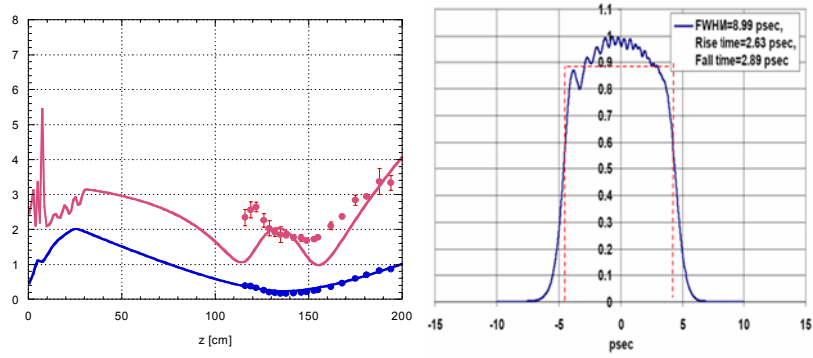


Figure 20. On the left hand side measured envelope (blue dots) and emittance (red dots) and Homdyn results (continuous lines). On the right hand side corresponding measured pulse and Homdyn model.

Table 7. Measured parameters.

Parameter	Value
Energy	5.65 MeV
Charge	825pC
Spot size, $\langle\sigma\rangle$	$\langle\sigma_x\rangle=353\ \mu\text{m}$, $\langle\sigma_y\rangle=365\ \mu\text{m}$
RF phase, $\varphi-\varphi_{\text{max}}$	-8°
Solenoid current	209 A

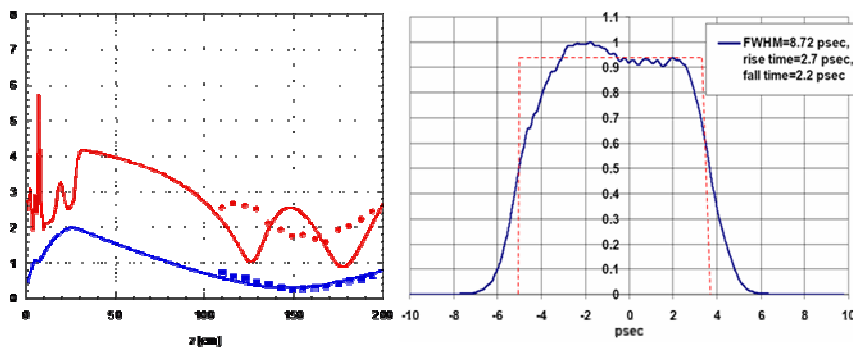


Figure 21. On the left hand side measured envelope (blue dots) and emittance (red dots) and Homdyn results (continuous lines). On the right hand side corresponding measured pulse and Homdyn model.

Table 8. Measured parameters.

Parameter	Value
Energy	5.4 MeV
Charge	740 pC
Spot size, $\langle\sigma\rangle$	$\langle\sigma_x\rangle=297\ \mu\text{m}$, $\langle\sigma_y\rangle=322\ \mu\text{m}$
RF phase, $\varphi-\varphi_{\text{max}}$	-8°
Solenoid current	199 A

Figure 22 shows again a comparison between the measured envelope and emittance and Homdyn simulations. The difference is that the pulse is much more flat than the previous cases and the rise time is around 1psec. For these reasons the agreement is much more satisfactory.

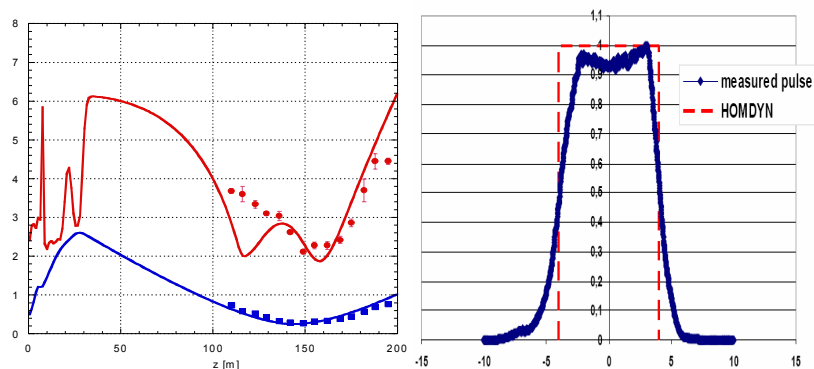


Figure 22. On the left hand side measured envelope (blue dots) and emittance (red dots) and Homdyn results (continuous lines). On the right hand side corresponding measured pulse and Homdyn model.

Table 9. Measured parameters.

Parameter	Value
Energy	5.6 MeV
Charge	1nC
Spot size, $\langle\sigma\rangle$	$\langle\sigma_x\rangle=388\ \mu\text{m}$, $\langle\sigma_y\rangle=394\ \mu\text{m}$
RF phase, $\varphi-\varphi_{\text{max}}$	0°
Solenoid current	209 A
Pulse length (FWHM)	8 ps

Finally the short pulse rise time, shown on the right hand side of figure 23, allowed the measure of the double minimum described previously. On the left hand side a comparison between the measured emittance, the Parmela fit and Homdyn result is shown. The pulse is not perfectly flat, thus the fitting procedure had to be forced more than the previous case; as expected Homdyn evidences a deeper oscillation due to the non perfect uniformity of the charge distribution inside the pulse.

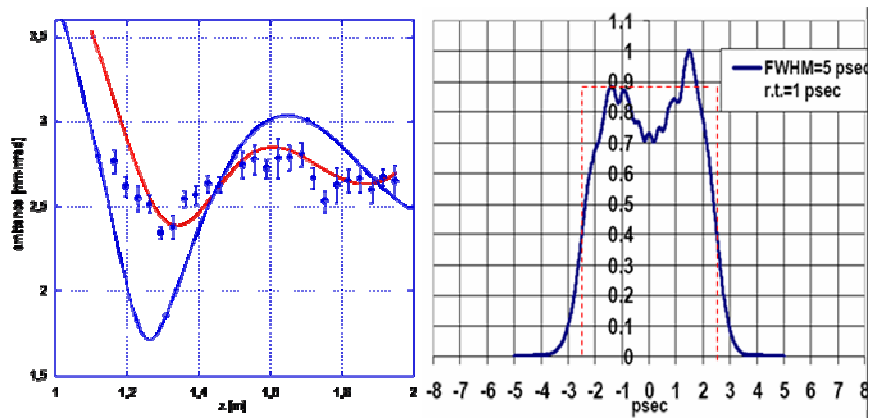


Figure 23. On the left hand side measured emittance (blue dots), Parmela fit (red continuous line) and Homdyn result (blue continuous lines). On the right hand side corresponding measured pulse and Homdyn model.

Table 10. Measured parameters.

Parameter	Value
Energy	5.5 MeV
Charge	500 pC
Spot size, $\langle\sigma\rangle$	450 μm
RF phase, $\varphi - \varphi_{\text{max}}$	12°
Solenoid current	198 A

As last comparisons Figure 24 and 25 shows the measured energy spread and the Homdyn fit.

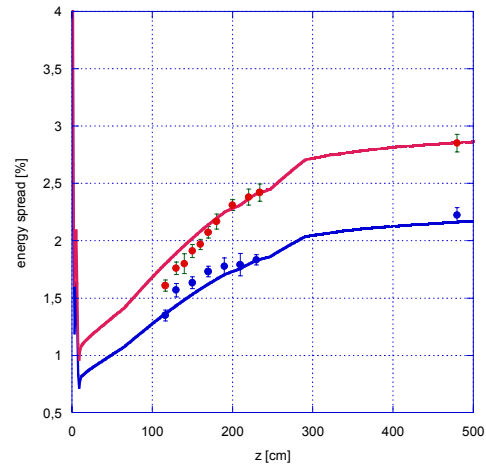


Figure 24. Measured energy spread and Homdyn simulations for 360 pC (red dots and line) and for 200 pC (blue dots and line).

Table 11. Measured parameters.

Parameter	Value
Energy	5.5 MeV
Spot size, $\langle\sigma\rangle$	450 μm
RF phase, $\varphi - \varphi_{\text{max}}$	12°
Solenoid current	195 A
Pulse length (FWHM)	5 psec

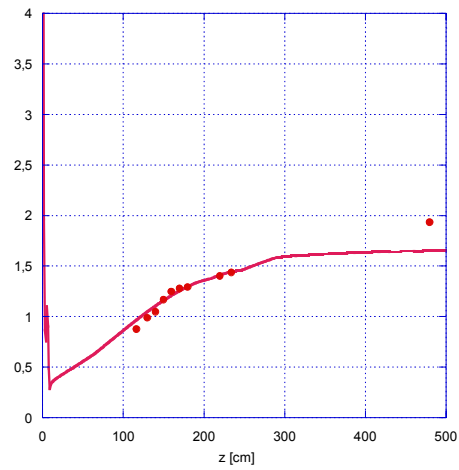


Figure 24. Measured energy spread and Homdyn simulations for 360 pC

Table 11. Measured parameters.

Parameter	Value
Energy	5.5 MeV
Spot size, $\langle\sigma\rangle$	450 μm
RF phase, $\varphi-\varphi_{\text{max}}$	0°
Solenoid current	185 A
Pulse length (FWHM)	5 psec

Wake fields in the emittance meter have been studied as well [16]. For an emittance meter 1.5 m long, considered as a unique piece of structure, the obtained energy spread is shown on the left hand side of Figure 25, whilst the right hand side represents the emittance variation in percent as a function of the bellow misalignment.

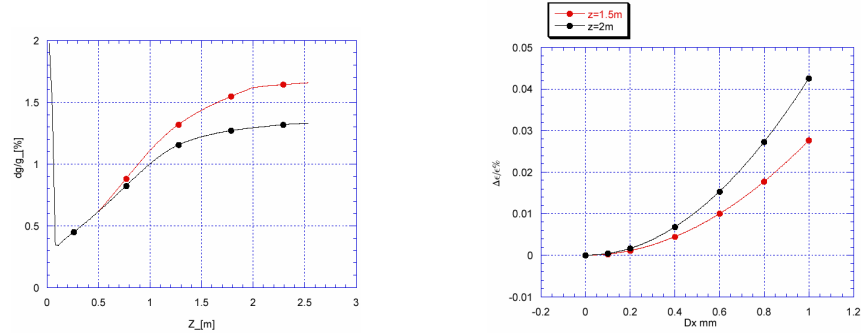


Figure 25.(Left hand side) Energy spread vs z with and without bellow structure as computed by Homdyn. (Right hand side) Emittance degradation in percent vs Δx , the bellow structure misalignment. Both plots have been obtained for Sparc nominal parameters [17].

The energy spread blowup can be neglected and in the worst case of 1 mm misalignment, the contribution of the wakes to the emittance degradation is less than 0.05%. These results have been confirmed by the excellent agreement between measurements and Parmela code [15] which doesn't take into account wake fields.

7. Conclusions

The Homdyn model has been described together with its improvements: off axis beam dynamics has been included in the code allowing the study of wake fields.

In fact wake fields, besides space charge and RF fields, may have an important impact in the emittance compensation process.

The analytical formula used for the wake fields has been described: wake fields for a single cavity, in the diffraction model limit, and wake fields for a periodic structure, for the SLAC type cavity, can be considered in the Homdyn computation.

Comparisons between Homdyn and analytical calculations, concerning the energy spread and the offset induced by wake fields, has been also discussed together with the description of the emittance, calculated using its statistical definition.

Homdyn allowed the study and the project of the steering magnets positions; the choice proposed is an example of emittance compensation process strongly influenced by wake fields.

The code has been applied to the emittance-meter of the SPARC project to evaluate the energy spread and the emittance compared with the measurements.

References (da completare)

1. M. Ferrario et al., Proc. of The Physics and Application of High Brightness Electron Beams (2002).
2. M. Ferrario et al., Proc. of The Physics and Application of High Brightness Electron Beams (2000).
3. M. Reiser, Theory and design of charged particle beams, Wiley-Interscience Pub. (1994).
4. V. Fusco, Beam dynamics and collective effects in the Sparc project, PhD thesis (2005).
5. L. Palumbo et al., Wake fields and impedante, Proc. of CAS (1993).
6. J. Lawson, Rutherford High Energy Laboratory Report, RHEL/M144 (1968).
7. K. Bane, M. Sands, Wake fields of very short bunches in an accelerating cavity(2001), Proc. Of Workshop on Impedance Beyond cut off (1987).
8. V. Fusco et al., Wake fields effects in the Sparc photo-injector, Proc. of EPAC (2004).
9. K. Bane, SLAC-PUB 9663, (2003).
10. R. B. Palmer, A qualitative study of wake fields for very short bunches, Tech. Rep. BNL (1987).
11. V. Fusco et al., Wake fields effects in the SPARC linac, Proc. of SPIE (2004).
12. J. Buon, Beam phase space and emittance, Proc. of CAS (1992).
13. L. Serafini, J. B. Rosenzweig, Phys. Rev. E **5**, 7565 (1997)
14. L. Catani et al., Review of Scientific Instruments **77**, 93301 (2006)
15. C. Ronsivalle et al., in Proceedings of PAC07, Albuquerque (New Mexico)

16. V. Fusco et al., in Proc. Of the ICFA Workshop, Erice, October 2005, World Scientific
17. D. Alesini et al. Nucl. Instr. & Meth. In Phys. Res. A **507**, 345 (2003)